Xiangyu Li
School of Mechanical Engineering;
Birck Nanotechnology Center,
Purdue University,
West Lafayette, IN 47907
e-mail: li1215@purdue.edu

Wonjun Park
School of Electrical and Computer Engineering;
Birck Nanotechnology Center,
Purdue University,
West Lafayette, IN 47907
e-mail: wjpark249@gmail.com

Yong P. Chen
Department of Physics and Astronomy;
Birck Nanotechnology Center;
School of Electrical and Computer Engineering,
Purdue University,
West Lafayette, IN 47907
e-mail: yongchen@purdue.edu

Xiulin Ruan
School of Mechanical Engineering;
Birck Nanotechnology Center,
Purdue University,
West Lafayette, IN 47907
e-mail: ruan@purdue.edu

Effect of Particle Size and Aggregation on Thermal Conductivity of Metal–Polymer Nanocomposite

Metal nanoparticle has been a promising option for fillers in thermal interface materials due to its low cost and ease of fabrication. However, nanoparticle aggregation effect is not well understood because of its complexity. Theoretical models, like effective medium approximation model, barely cover aggregation effect. In this work, we have fabricated nickel–epoxy nanocomposites and observed higher thermal conductivity than effective medium theory predicts. Smaller particles are also found to show higher thermal conductivity, contrary to classical models indicate. A two-level effective medium approximation (EMA) model is developed to account for aggregation effect and to explain the size-dependent enhancement of thermal conductivity by introducing local concentration in aggregation structures. [DOI: 10.1115/1.4034757]

Introduction

Including metal nanoparticles in polymers, such as epoxy, helps to enhance thermal conductivity and to maintain electrical insulation below percolation threshold. Because of the low cost of fabrication, metal–epoxy composite has been a great option for thermal interfacial material in many applications [1]. Aggregation effect is often observed in nanocomposites and attributed as a dominant factor in thermal conductivity enhancement [2–10]. However, its complex morphology posts a great challenge for nanocomposite design and theoretical modeling.

To estimate overall thermal conductivity with fillers, many effective medium approximation models are proposed and reviewed [11–13]. The Maxwell model assumes isolated and spherical particles in matrix material, neglecting any interactions between particles [14,15]. Several modifications, such as the Hamilton model [16] and modified effective medium approximation [17], include a geometry factor of fillers, interfacial resistance and size effect both in filler and matrix material. Utilizing Green's function, Nan has developed a model that treats filler aspect ratio, orientation, and interfacial resistance [18]. However, these models only consider isolated particles, while aggregation effect remains neglected. The series and parallel models [19] consider the most simplified geometry of multifilm stacked together. The Bruggeman model [20] was developed for powder compact, and it neglects the effect of continuous phase of the matrix material. Therefore, the Bruggeman model provides a much lower thermal conductivity when interfacial resistance is considered. The percolation model [21] for thermal conductivity does include interactions between particles and distinguish particles and matrix, with percolation threshold and percolation exponent as two fitting parameters. Compared with electrical properties in metal–polymer composites, thermal transport does not show an increase in conductivity as dramatic as electrical conductivity [21–23]. Thus, fitting parameters can be sensitive to experimental data. Some methods for nanofluid utilize hierarchical EMA models to include the aggregation effect [24] by using fractal dimensions, which can be difficult to determine [22,25,26] especially for nanocomposite. The backbone method is another three-level homogenization model developed by Prasher et al. [27,28]. It relies on two predetermined fractal dimensions. However, it still fails to fit against our experimental data of nanocomposites. Other modeling methods, such as Monte Carlo, Boltzmann transport equation (BTE), or molecular dynamics (MD), are limited to simple periodic geometries due to their high-computing cost [29].

In our work, we have fabricated nickel nanoparticle–epoxy nanocomposites and observed that they show higher thermal conductivity than effective medium theory predicts even at low concentrations below the percolation threshold. Furthermore, larger enhancement in thermal conductivity is obtained with smaller nanoparticles at the same concentration, contrary to what classical EMA models predict. Thermal conductivity characterization is done by 3ω method, and microscopy analysis by transmission electron microscopy (TEM) indicates thermal conductivity enhancement and size-dependency are caused by the aggregation effect. A two-level effective medium approximation model is developed to consider inhomogeneous dispersion of nanoparticles, by distinguishing local and global concentrations. A rough estimation of the local concentration can be also gained with TEM figures, matching reasonably well with modeling results. Overall, the new two-level EMA model helps explain aggregation effect in nanocomposite and the size-dependent thermal conductivity enhancement, which other EMA models fail to explain.

Sample Fabrication

Nickel particles of multiple sizes 10 nm (9.9 ± 0.2 nm), 40 nm (37.1 ± 2.2 nm), 70 nm (67.5 ± 2.5 nm), and 1 μm (0.86 ± 0.09 μm) are used to make nanocomposites. 10 nm nickel particles are purchased through mkNano Inc., Missisauga,

Canada, and other nickel particles are from Skyspring Nanomaterials, Houston, TX. Matrix materials consist of epon 862, epikure W, both purchased from Miller-Stephenson, Morton Grove, IL, and curing accelerator epikure 3253 for preventing particle precipitation provided by Matteson-Ridolfi, Inc., Riverview, MI. Nickel particles, epoxy resin, curing agent, and accelerator are mixed together in THINKY mixer ARE-310 for 10 min. The mixture is degassed for 1 h, then poured into aluminum mold. Releasing agents are sprayed ahead of time to ensure an easier removal of samples. The curing procedure occurs in an oven, with 30 min temperature ramp from room temperature to 121 °C with 2 h hold, followed by a 30 min ramp from 121 °C to 177 °C and 2 h hold, and then a slow cooldown to room temperature [30].

The samples produced are pellets of 2.5 mm thickness and 1.5 cm in diameter. The top and bottom surfaces are polished to avoid contamination from releasing agent and to make the surfaces smooth for 3ω measurements. The density is measured before and after polishing to ensure that the volume concentration of nickel is consistent.

Thermal Conductivity Characterization

Thermal conductivity is measured by the 3ω method [31,32]. It requires a thin metal line on the surface of the sample, functioning both as a heater and detector. A metal line of 4 mm long and 40 μm wide is deposited on the surface of the sample with shadow mask, consisting of 20 nm Cr and 150 nm Au. Because of the microscale size of the metal line, radiation loss even at high temperature is insignificant. There have been different variations of this method to measure thin films, fluid, multilayer films, anisotropic thermal conductivity materials, etc. [33,34]. During the measurement, an AC current of frequency ω is applied to the metal line, heating up the surface of the sample with a temperature oscillation amplitude ΔT. A voltage of 3ω frequency is also present across the metal line. Detailed deductions about ΔT can be found in previous literatures [31,32] as

$$\Delta T = \frac{2v_{3\omega}}{v_{1\omega}C_{\mathrm{rt}}} = \frac{p}{\pi k}\int_0^\infty \frac{\sin^2(\lambda b)}{(\lambda b)^2(\lambda^2 + 2i\omega/D)^{1/2}}d\lambda \qquad (1)$$

By measuring $v_{1\omega}$, $v_{3\omega}$, and temperature coefficient of resistance C_{rt} of the metal line, thermal conductivity of nanocomposites can be obtained by fitting real and imaginary part of theoretical $\Delta T/p$ to experimental in-phase and out-of-phase signal, respectively. A typical fitting procedure on one of our Ni–epoxy nanocomposite samples is shown in Fig. 1, with thermal conductivity obtained as 0.28 W/m K. The thermal penetration depth is around 25 μm at 5 Hz, 5 μm at 100 Hz, and 1.3 μm at 2000 Hz, while the largest size scale of the inhomogeneity due to aggregations is 1–3 μm as seen in Fig. 2(b) (Fig. 2(a) shows smaller inhomogeneity scale). Besides, the inhomogeneity is also averaged across the metal line (4 mm × 40 μm), which is large enough to obtain an effective thermal conductivity of the sample.

The thermal conductivities of nanocomposites with different nickel particle sizes and volume concentrations are shown in Fig. 3, where the Maxwell model curve is also plotted. Without the inclusion of interfacial resistance, the thermal conductivity from the Maxwell model is independent on particle sizes. All of the thermal conductivities are higher than the Maxwell model predicts. Surprisingly, it is also observed that smaller fillers provide higher thermal conductivity at the same concentration, contrary to the trend of classical EMA models, where thermal conductivity decreases with smaller particles due to interfacial resistance. Motivated by these observations, we slice our composites' samples into 100 nm thickness and characterize the microscopy structure with transmission electron microscopy (TEM). According to Fig. 2, nickel particles (dark dots) are not isolated or located evenly. Instead, they aggregate to form some clusters with high-local concentration. Interactions between particles help form a
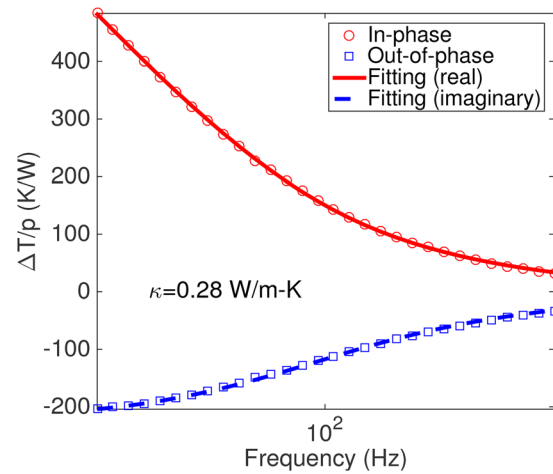

Fig. 1 In-phase and out-of-phase 3ω signals (hollow circles and squares) are fitted with analytical solution (solid line and dashed line) to obtain thermal conductivity of Ni–epoxy nanocomposites

continuous path to conduct heat better within nickel phase, thus increase the overall thermal conductivity more effectively than isolated dispersion. On the other hand, these clusters are mostly isolated from each other. It is also important to note that 40 nm nanoparticles form a more spread-out cluster structure than 70 nm, which is likely the reason for size-dependent thermal conductivity. In this case, using a single-level EMA model like the Maxwell model would ignore the aggregation effect. On the other hand, although the percolation model considers the aggregation effect, it does not treat the nonuniform particle distribution. In this work, a two-level EMA is developed to account for the aggregation effect.

Two-Level EMA Modeling

Our two-level EMA model adopts a different EMA model at each level, shown in Fig. 4. The first level is a cluster where nanoparticles are packed closely, and the second level is the whole composite where each cluster is treated as an isolated new particle. A local concentration, ϕ_l, is defined as the volume concentration of particles inside clusters. The cluster concentration, ϕ_c, is defined as volume concentration of clusters inside the matrix material. Thus, the overall concentration of nanoparticles will be preserved as $\phi = \phi_l \times \phi_c$. For the first level EMA, where particles are packed together, the Hashin and Shtrikman model [35] is used as

$$k_{c,o} = k_p \frac{2\phi_l}{3 - \phi_l} \qquad (2)$$

where k_p is nickel particle thermal conductivity, ϕ_l is the local volume concentration, and $k_{c,o}$ is the thermal conductivity of clusters neglecting interface resistance. Several attempts in literature have shown that with sufficient particle interactions at high concentration, thermal conductivity enhancement can be comparable to the higher bound of the Hashin and Shtrikman model [5–9,36]. Thermal interface resistance between epoxy and nickel particles can also be included as [37]

$$\frac{1}{k_c} = \frac{1}{k_{c,o}} + \frac{2R_i}{d} \qquad (3)$$

where k_c is the thermal conductivity of clusters considering interfacial resistance, R_i is the thermal interfacial resistance, and d is the diameter of nickel particles. The interfacial resistance is added in the same manner that it is included for isolated spheres [18]. However, aggregation and sintering effects shown in Fig. 5
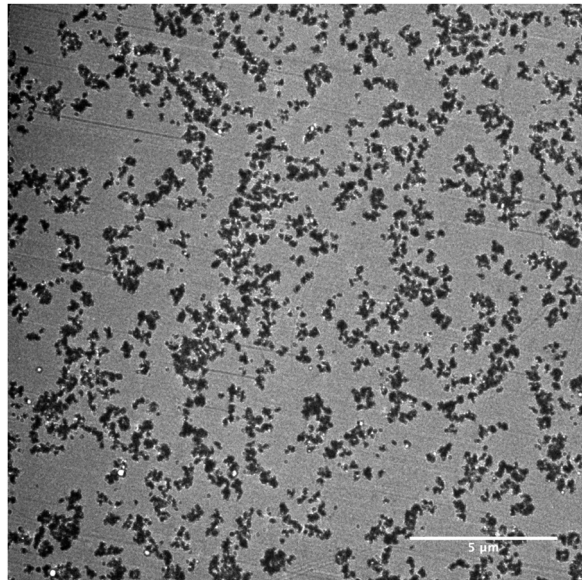
(a)
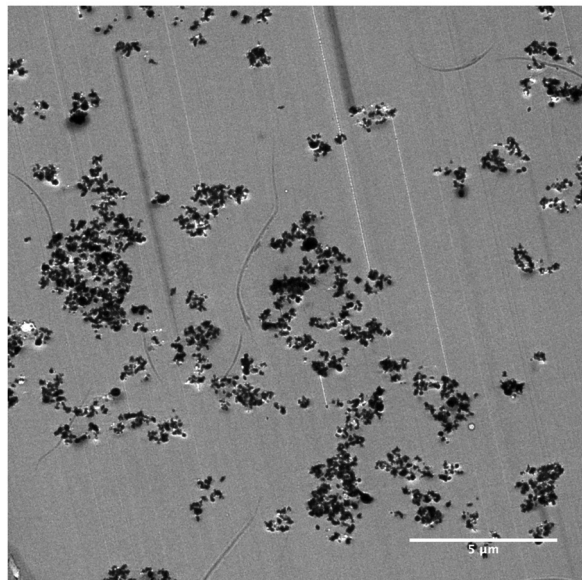
(b)

Fig. 2 TEM figures of nanocomposites with 40 nm and 70 nm nickel particles are taken at the same magnification, scale bar set as 5 μm for (a) and (b). A more spread-out aggregation structure is observed in nanocomposites with smaller particle size than that in larger one at similar concentrations.

decrease the surface area significantly and change the shape of clusters [36], resulting in a diminished effect of thermal interfacial resistance on overall thermal conductivity. Thus, simply applying R_i and the diameter of individual particles as d will overestimate the effect of interfacial resistance. Due to its complexity, another model is needed to quantify the exact effect of interfacial resistance due to the agglomerations. On the second level, even though the aggregation structures appear as cylinders, rods, and some irregular shapes in TEM images, the true geometry factor remains uncertain. The TEM figures only show a slice of 100 nm thickness, thus those agglomerations that seem to be connected together might be relatively distant away, and some small agglomerations might be only part of larger ones. Because of spherical particles and isolated clusters, we assume spherical agglomerations based on the Maxwell model as
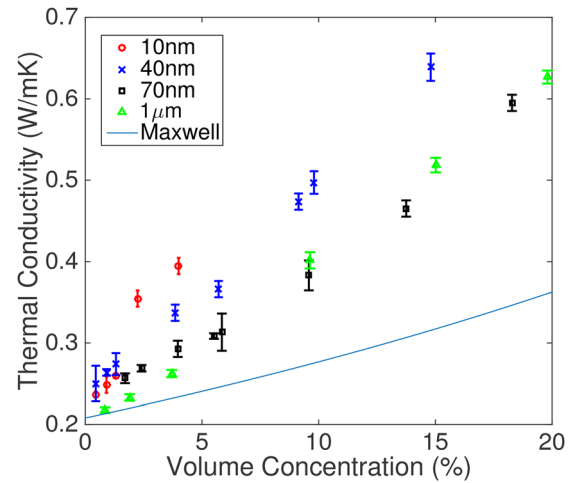

Fig. 3 Thermal conductivities of Ni–epoxy composites with different particle sizes and concentrations are compared with the Maxwell model. All thermal conductivities are higher than the Maxwell model, and smaller particles yield higher thermal conductivities than larger ones. (a) Nanocomposite with 40 nm Ni at 5.74% and (b) nanocomposite with 70 nm Ni at 5.52%.
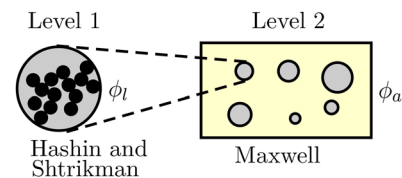

Fig. 4 Two-level EMA model applied two different EMA models to calculate thermal conductivities of the clusters (level 1) and the overall composite (level 2)

$$k_e = k_m \frac{k_c + 2k_m + 2\phi_c(k_c - k_m)}{k_c + 2k_m - \phi_c(k_c - k_m)} \quad (4)$$

where k_c is the thermal conductivity of clusters, k_e is the effective thermal conductivity of nanocomposites, k_m is the matrix thermal conductivity, and ϕ_c is the volume concentration of clusters in epoxy. In this work, thermal interface resistance is set to be 5×10^{-9} m² K/W [38]. We applied a constant interfacial resistance between nickel and epoxy, although it is reported that interfacial resistance may vary depending on particle sizes [38]. The thermal conductivity of nickel particles is estimated based on the mean free path of phonons and the electron cooling length [39], shown in Table 1. If the aspect ratio is to be measured or fitted in the model, Nan's model can be an alternative model to include the geometry factor.

The local concentration ϕ_l of each sample is an exact fit with experimental thermal conductivity data based on the two-level EMA model in Fig. 6, where the curve $\phi_l = \phi$ is also included for comparison. All local concentrations are above the curve $\phi_l = \phi$, indicating higher local concentrations in clusters. For smaller particles as 10 nm, 40 nm, and 70 nm at low concentrations, the local concentration increases faster than overall concentration does. In other words, particles tend to aggregate more closely with higher particle loadings. After certain concentration, the local concentration increasing speed becomes similar to that of overall concentration. It is interesting to note that with a lower local concentration, the overall thermal conductivity tends to be higher at the same overall concentration. A comparison is made between 40 nm sample at 5.74% and 70 nm sample at 5.52% in Table 2. Even though 70 nm nanocomposite has a higher local concentration, thus a
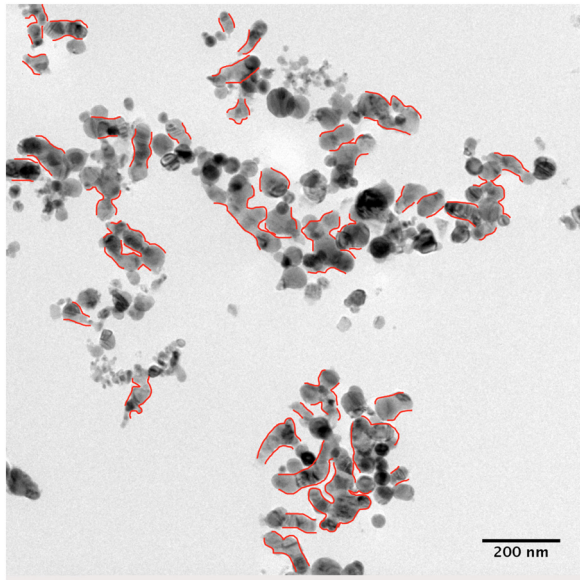
Fig. 5 Sintering effect is observed in nanocomposite with 40 nm Ni at 5.74%. Lines are labeled where a continuous path is formed among nanoparticles. The scale bar is set as 200 nm.

Table 1 Thermal conductivity of nickel particles with size effect

Particle size	10 nm	40 nm	70 nm	1 μm
Thermal conductivity (W/m K)	36.7	66.0	74.5	90.9

higher cluster thermal conductivity, its lower cluster concentration limits its overall thermal conductivity. Referring to Fig. 2 at similar concentrations and the same magnification, the aggregation structure of 40 nm nanoparticles is more beneficial for heat transfer, since clusters are more spread-out, which translates into larger ϕ_c or smaller ϕ_l. Thus, the aggregation effect enhances thermal conductivity compared with isolated particle dispersion, and an extensive aggregation structure or low-local concentration is preferred for higher thermal conductivity. The local concentration of the composites with 1 μm nickel particles is less dependent on overall concentration mainly because of its much larger size compared with other nanoparticles, thus smaller number of particles and longer distance between them.

Besides fitting to the thermal conductivities of experimental data, the local concentrations of nickel particles in clusters can also be roughly estimated from TEM images by evaluating cluster concentration in matrix ϕ_c first. The method is to assume the particle distribution to be uniform along with the 100 nm thickness of TEM slice. Then, the ratio of area occupied by closely packed particle to the total area is ϕ_c. Using the overall concentration of particles ϕ, the local concentration ϕ_l can be estimated. Figure 2 contains two TEM pictures of 40 nm nickel and 70 nm nickel at similar volume concentrations. The local concentration of these two samples are calculated to be $13.1\% \pm 0.2\%$ and $23.9\% \pm 1.8\%$, respectively, comparing to the fitted local concentrations 23% and 35%. This is probably because that the assumption that the particle dispersion is uniform across 100 nm overestimates ϕ_c, thus underestimates ϕ_l. Nonetheless, the estimations based on the TEM images still follow the same trend with those fitted from our two-level EMA model.

The backbone method is another hierarchical EMA model, proposed by Prasher et al., estimating thermal conductivity of nanofluid including the aggregation effect [27,28]. Three
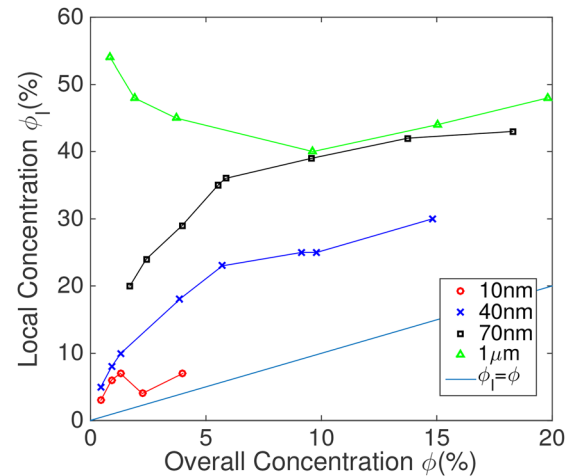

Fig. 6 Local concentration of Ni particles in aggregations is plotted with different overall concentrations and nickel particle sizes

Table 2 Comparison between two nanocomposites

Particle size (nm)	ϕ (%)	ϕ_l (%)	ϕ_c (%)	k_c (W/m K)	k_e (W/m K)
40	5.74	23	25.0	11.1	0.37
70	5.52	35	15.8	19.9	0.31

parameters are needed as overall fractal dimension, backbone fractal dimension, and gyration radius. Overall fractal dimension is usually set as 1.7 for nanofluids and 2.0 for nanocomposites [25,26]. However, the model cannot achieve thermal conductivity as high as our experimental results, even by setting gyration radius as a parameter.

Conclusion

In this work, we observe higher thermal conductivity of nickel–epoxy nanocomposites compared with other EMA models predict, due to aggregation effect. At the same concentration, smaller particle size shows higher thermal conductivities due to its wider-spread aggregation structures in epoxy, according to TEM figures. A two-level EMA model with the local concentration as a fitting parameter indicates a lower local concentration for smaller particles, thus a higher effective thermal conductivity. The local concentration for nanoparticles also shows an increasing trend with higher overall concentration and saturates later. An estimation of local concentration based on TEM figures follows the trend and agrees reasonably well with modeling results. Overall, the new two-level EMA model works well with nanocomposites and helps explain the aggregation effect and size-dependent thermal conductivity enhancement.

Nomenclature

b = half width of metal line
C_{rt} = coefficient between resistance and temperature
D = thermal diffusivity
k = thermal conductivity
k_c = cluster thermal conductivity

k_e = overall thermal conductivity
k_m = matrix thermal conductivity
k_p = particle thermal conductivity
p = power consumption of metal line in 3ω measurement
q^{-1} = penetration depth
$v_{1\omega}$ = voltage signal of ω frequency
$v_{3\omega}$ = voltage signal of 3ω frequency
ΔT = temperature oscillation amplitude
ϕ = volume concentration
ϕ_c = cluster concentration in matrix
ϕ_l = local volume concentration in agglomeration
ω = frequency of current in 3ω measurement

References

[1] Ellis, B., 1993, *Chemistry and Technology of Epoxy Resins*, Blackie Academic & Professional, New York.
[2] Hsu, S. H., Chou, C. W., and Tseng, S. M., 2004, "Enhanced Thermal and Mechanical Properties in Polyurethane/Au Nanocomposites," Macromol. Mater. Eng., **289**(12), pp. 1096–1101.
[3] Karthikeyan, N., Philip, J., and Raj, B., 2008, "Effect of Clustering on the Thermal Conductivity of Nanofluids," Mater. Chem. Phys., **109**(1), pp. 50–55.
[4] Pardiñas-Blanco, I., Hoppe, C. E., López-Quintela, M., and Rivas, J., 2007, "Control on the Dispersion of Gold Nanoparticles in an Epoxy Network," J. Non-Cryst. Solids, **353**(8–10), pp. 826–828.
[5] Philip, J., Shima, P. D., and Raj, B., 2008, "Evidence for Enhanced Thermal Conduction Through Percolating Structures in Nanofluids," Nanotechnology, **19**(30), p. 305706.
[6] Philip, J., Shima, P. D., and Raj, B., 2008, "Nanofluid With Tunable Thermal Properties," Appl. Phys. Lett., **92**(4), pp. 2–5.
[7] Philip, J., Shima, P. D., and Raj, B., 2007, "Enhancement of Thermal Conductivity in Magnetite Based Nanofluid Due to Chainlike Structures," Appl. Phys. Lett., **91**(20), pp. 2–5.
[8] Reinecke, B. N., Shan, J. W., Suabedissen, K. K., and Cherkasova, A. S., 2008, "On the Anisotropic Thermal Conductivity of Magnetorheological Suspensions," J. Appl. Phys., **104**(2), p. 023507.
[9] Wu, S., Ladani, R. B., Zhang, J., Kinloch, A. J., Zhao, Z., Ma, J., Zhang, X., Mouritz, A. P., Ghorbani, K., and Wang, C. H., 2015, "Epoxy Nanocomposites Containing Magnetite-Carbon Nanofibers Aligned Using a Weak Magnetic Field," Polymer, **68**, pp. 25–34.
[10] Zhu, H., Zhang, C., Liu, S., Tang, Y., and Yin, Y., 2006, "Effects of Nanoparticle Clustering and Alignment on Thermal Conductivities of Fe_3O_4 Aqueous Nanofluids," Appl. Phys. Lett., **89**(2), p. 023123.
[11] Lee, J.-H., Lee, S.-H., Choi, C. J., Jang, S. P., and Choi, S. U. S., 2011, "A Review of Thermal Conductivity Data, Mechanisms and Models for Nanofluids," Int. J. Micro-Nano Scale Transp., **1**(4), pp. 269–322.
[12] Lee, S., Cahill, D. G., and Allen, T. H., 1995, "Thermal Conductivity of Sputtered Oxide Film," Phys. Rev. B, **52**(1), pp. 253–257.
[13] Wang, M., and Pan, N., 2008, "Predictions of Effective Physical Properties of Complex Multiphase Materials," Mater. Sci. Eng., R, **63**(1), pp. 1–30.
[14] Maxwell, J., 1954, *A Treatise on Electricity and Magnetism*, Dover Publications, Mineola, NY.
[15] Garnett, J. C. M., 1906, "Colours in Metal Glasses, in Metallic Films, and in Metallic Solutions. II," Philos. Trans. R. Soc., A, **205**(387–401), pp. 237–288.
[16] Hamilton, R. L., and Crosser, O. K., 1962, "Thermal Conductivity of Heterogeneous Two-Component Systems," Ind. Eng. Chem. Fundam., **1**(3), pp. 187–191.
[17] Minnich, A., and Chen, G., 2007, "Modified Effective Medium Formulation for the Thermal Conductivity of Nanocomposites," Appl. Phys. Lett., **91**(7), p. 073105.
[18] Nan, C.-W., Birringer, R., Clarke, D. R., and Gleiter, H., 1997, "Effective Thermal Conductivity of Particulate Composites With Interfacial Thermal Resistance," J. Appl. Phys., **81**(10), pp. 6692–6699.
[19] Eucken, A., 1932, "Thermal Conductivity of Ceramic Refractory Materials: Calculation From Thermal Conductivities of Constituents," Ceramic Abstracts, Vol. 11.
[20] Landauer, R., 1952, "The Electrical Resistance of Binary Metallic Mixtures," J. Appl. Phys., **23**(7), pp. 779–784.
[21] Zhang, G., Xia, Y., Wang, H., Tao, Y., Tao, G., Tu, S., and Wu, H., 2010, "A Percolation Model of Thermal Conductivity for Filled Polymer Composites," J. Compos. Mater., **44**(8), pp. 963–970.
[22] Nan, C.-W., 1993, "Physics of Inhomogeneous Inorganic Materials," Prog. Mater. Sci., **37**(1), pp. 1–116.
[23] Nan, C.-W., Shen, Y., and Ma, J., 2010, "Physical Properties of Composites Near Percolation," Annu. Rev. Mater. Res., **40**(1), pp. 131–151.
[24] Wang, B. X., Zhou, L. P., and Peng, X. F., 2003, "A Fractal Model for Predicting the Effective Thermal Conductivity of Liquid With Suspension of Nanoparticles," Int. J. Heat Mass Transfer, **46**(14), pp. 2665–2672.
[25] Meakin, P., Majid, I., Havlin, S., and Stanley, H. E., 1999, "Topological Properties of Diffusion Limited Aggregation and Cluster–Cluster Aggregation," J. Phys. A: Math. Gen., **17**(18), pp. L975–L981.
[26] Meakin, P., 1987, "Fractal Aggregates," Adv. Colloid Interface Sci., **28**, pp. 249–331.
[27] Prasher, R., Evans, W., Meakin, P., Fish, J., Phelan, P., and Keblinski, P., 2006, "Effect of Aggregation on Thermal Conduction in Colloidal Nanofluids," Appl. Phys. Lett., **89**(14), pp. 1–4.
[28] Evans, W., Prasher, R., Fish, J., Meakin, P., Phelan, P., and Keblinski, P., 2008, "Effect of Aggregation and Interfacial Thermal Resistance on Thermal Conductivity of Nanocomposites and Colloidal Nanofluids," Int. J. Heat Mass Transfer, **51**(5–6), pp. 1431–1438.
[29] Chen, G., 1998, "Thermal Conductivity and Ballistic-Phonon Transport in the Cross-Plane Direction of Superlattices," Phys. Rev. B, **57**(23), pp. 14958–14973.
[30] Chen, C., and Curliss, D., 2003, "Preparation, Characterization, and Nanostructural Evolution of Epoxy Nanocomposites," Appl. Polym. Sci., **90**(8), pp. 2276–2287.
[31] Cahill, D. G., 1990, "Thermal Conductivity Measurement From 30 to 750 K: The 3ω Method," Rev. Sci. Instrum., **61**(2), pp. 802–808.
[32] Cahill, D. G., 1989, "Thermal Conductivity of Thin Films: Measurements and Understanding," J. Vac. Sci. Technol., A, **7**(3), pp. 1259–1266.
[33] Bodenschatz, N., Liemert, A., Schnurr, S., Wiedwald, U., and Ziemann, P., 2013, "Extending the 3ω Method: Thermal Conductivity Characterization of Thin Films," Rev. Sci. Instrum., **84**(8), p. 084904.
[34] Borca-Tasciuc, T., Kumar, A. R., and Chen, G., 2001, "Data Reduction in 3ω Method for Thin-Film Thermal Conductivity Determination," Rev. Sci. Instrum., **72**(4), pp. 2139–2147.
[35] Hashin, Z., and Shtrikman, S., 1962, "A Variational Approach to the Theory of the Effective Magnetic Permeability of Multiphase Materials," J. Appl. Phys., **33**(10), pp. 3125–3131.
[36] Pashayi, K., Fard, H. R., Lai, F., Iruvanti, S., Plawsky, J., and Borca-Tasciuc, T., 2012, "High Thermal Conductivity Epoxy-Silver Composites Based on Self-Constructed Nanostructured Metallic Networks," J. Appl. Phys., **111**(10), p. 104310.
[37] Toprak, M., Stiewe, C., Platzek, D., Williams, S., Bertini, L., Muller, E., Gatti, C., Zhang, Y., Rowe, M., and Muhammed, M., 2004, "The Impact of Nanostructuring on the Thermal Conductivity of Thermoelectric $CoSb_3$," Adv. Funct. Mater., **14**(12), pp. 1189–1196.
[38] Ong, W.-L., Majumdar, S., Malen, J. A., and McGaughey, A. J. H., 2014, "Coupling of Organic and Inorganic Vibrational States and Their Thermal Transport in Nanocrystal Arrays," J. Phys. Chem. C, **118**(14), pp. 7288–7295.
[39] Wang, Y., Ruan, X., and Roy, A. K., 2012, "Two-Temperature Nonequilibrium Molecular Dynamics Simulation of Thermal Transport Across Metal-Nonmetal Interfaces," Phys. Rev. B, **85**(20), p. 205311.